Steel and Composite Structures, Vol. 9, No. 6 (2009) 519-534
DOI: http://dx.doi.org/10.12989/scs.2009.9.6.519

An experiment on compressive profile of the unstiffened steel plate-concrete structures under compression loading

Choi, Byong Jeong† and Han, Hong Soo*

Department of Architectural Engineering, Kyonggi University, Seoul, Korea

(Received February 25, 2009, Accepted October 20, 2009)

Abstract. This study intends to examine the characteristics of compressive behavior and conducts comparative analysis between normal compressive strength under existing equations (LRFD, ACI 318, EC 4) and experimental the maximum compressive strength from the compression experiment for the unstiffened steel plate-concrete structures. The six specimens were made to evaluate the constraining factor (ξ) and width ratio (β) effects subjected to the compressive monotonic loading. Based on this experiments, the following conclusions could be made: first, compressive behaviors of the specimens from the finite element analysis closely agreed with the ones from the actual experiments; second, the higher the width ratio (β) was, the lower the ductility index (DI) was; and third, the test results showed the maximum compressive strength with a margin by 7% compared to the existing codes.

Keywords : composite column(s); steel plate-concrete; initial stiffness; ductility index; ultimate strength; finite element analysis.

1. Introduction

Recently, buildings become larger and high-storied, while structural members of buildings become slender. For this reason, the requirement for a new system is ever increasing. The Bi-Steel system that can be used in the core of a structure was recently developed and actively used in Europe (CORUS 2003). On the other hand, the research on the SC (Steel Plate-Concrete) structure as a new system has been implemented in Japan (JEAG 4618 2005). The steel plates, studs and concrete are the main components to form the SC structures. Up to date, the research on the SC structures is not enough to be used in practice due to their complex structural behaviors. Especially, the compressive characteristics of the SC structures are not well established until now. In this paper, the presentation is focused on the compressive characteristics of the SC structures using various parameters such as constraining factors and width ratios. In this paper, the structural failure behavior, initial stiffness, ductility, strain, and the maximum compressive strength based on the experimental results are evaluated.

2. Experimental plan

The six specimens were used in this experimental works in total. The compressive strength of concrete

†Associate Professor, Email:bjchoi@kyonggi.ac.kr
*Ph.D.,Corresponding Author Research Fellow, Email: water1973@hanmail.net

mix proportion was 35 N/mm^2. The aggregate was mixed as shown in Table 1. The compressive strength was 42 N/mm^2 at 28 days after concrete casting. For a steel plate, two types of steel were used: SM 490 and SS 400 in thickness of 6 mm. The material characteristics of SM 490 and SS 400 are shown in Table 2. A head stud (hereafter, stud) was designed to be 8 mm in diameter and 71 mm in length. Thickness of a steel plate, spacing of studs, and dimensions of specimens are shown in Table 3.

Fig. 1 shows shape of the SS400-M (or SM490-M) specimen. To integrate a steel plate and concrete, studs were used. Three studs were installed at a level with the specimen and other 3 studs installed at right angles to it. Each of the studs at a level with the specimen was installed at a distance of 40mm from the specimen edges, and the other stud was installed in the center. The distance from the first stud lines to the upper edge is one half of the stud spacing. A flat bearing plate was used for load to be homogeneously distributed to steel plates and concrete.

In this experiment, the specimens were made to examine the characteristics of compressive behavior for each specimen with the constraining factor (ξ) and the width ratio (β) as parameters in Table 3. In this experimental study, the constraining factor (ξ) was introduced to demonstrate a composite action between a steel tube of a CFT column and filling concrete. According to a literature survey (Han 2002), the higher the constraining factor (ξ) of a rectangular CFT column was, the higher the maximum compressive strength of concrete as well as ductility was. In addition, a width ratio (β) was introduced in order to see changes in compressive strength of a CFT column when there are different width and thickness at a cross section of a rectangular CFT column. According to the experiment by L-H Han (Han 2002), as the width ratio (β) became higher, compressive strength and ductility were rapidly decreased after maximum compressive strength was reached. Therefore an experiment was conducted with a constraining factor (ξ) and a width ratio (β) as parameters in order to examine maximum

Table 1 Experimental results for concrete compressive strength and a mixing ratio

Compressive strength	W/C	slump	Unit quantity of aggregate			
			W	C	S	G
N/mm^2	%	mm	N/m^3	N/m^3	N/m^3	N/m^3
42	35.9	210	1422	4158	8191	8966

Table 2 Experimental results for tensile strength of steel

Type of steel	Yyield strength	Tensile strength	Modulus of elasticity	Yield ratio	Elongation
	N/mm^2	N/mm^2	N/mm^2	%	%
SS 400	274	432	2.0E5	63	37.6
SM 490	418	572	2.0E5	79	31.4

Table 3 Specimen table

No	Specimen	Steel plate thickness (t)	Spacing of studs	Dimensions of specimen			Constraining factor (ξ)	Width ratio (β)
				Thickness (d)	Width (b)	Height (h)		
		mm	mm	mm	mm	mm		
1	SS400-S	6	150	300	380	450	0.32	1.27
2	SS400-M	6	200	300	480	600	0.32	1.60
3	SS400-L	6	300	300	680	900	0.32	2.27
4	SM490-S	6	150	300	380	450	0.49	1.27
5	SM490-M	6	200	300	480	600	0.49	1.60
6	SM490-L	6	300	300	680	900	0.49	2.27

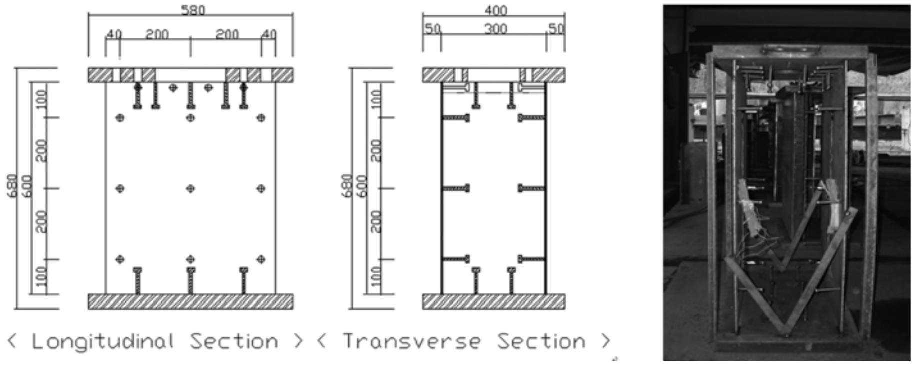

Fig. 1 Examples of specimen shape (SS400-M or SM490-M)

compressive strength and ductility of a USC compression member without lateral steel plate. A constraining factor (ξ) is shown in Eq. (1) and divided into two groups by 0.49 and 0.32 in this paper. A width ratio (β) is expressed in a width-to-thickness ratio of the specimen as shown in Eq. (2). Then the width ratio (β) is divided into 2.27, 1.60 and 1.27 in this experimental works.

$$\xi = \frac{F_y A_s}{0.85 f_c' A_c} \tag{1}$$

$$\beta = \frac{b}{d} \tag{2}$$

where, A_s : Cross-sectional area of steel plates, (mm^2)
A_c : Cross-sectional area of concrete, (mm^2)

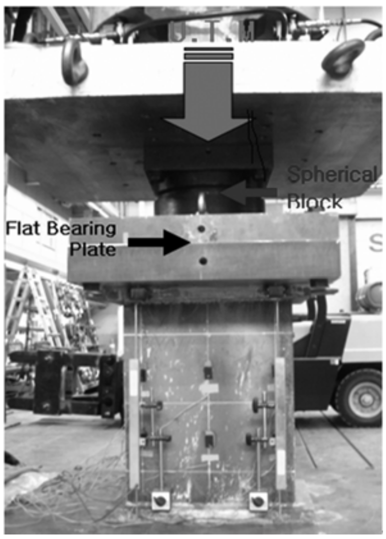

Fig. 2 Universal testing machine and specimen

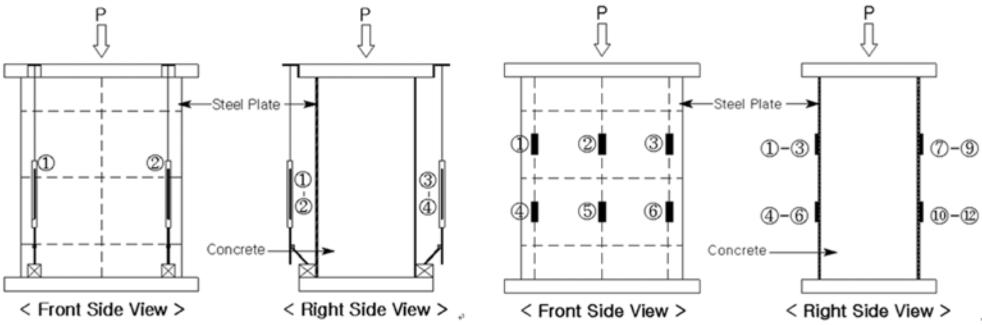

Fig. 3 Installation of measuring instrument

F_y : Yield strength of steel, (N/mm^2)
f_c' : Specified compressive strength of concrete, (N/mm^2)

For loading of specimens, the monotonic loading was applied unidirectionally to each specimen with a 10,000kN U.T.M (Universal Testing Machine). As shown in Fig. 2, a spherical block was installed on the top of a specimen to prevent eccentricity on the specimen. To observe axial displacement incurred on the specimen, LVDTs were installed. Pilot loading was given in the elasticity region that was less than 10% of the expected maximum compressive strength. Pivotal loading was conducted when the initial displacements from LVDT were observed with nearly same displacement each other. To observe strain of each material, strain gauges for the steel plates and the encased concrete were installed shown in Fig. 3. The purpose of LVDT installation is to measure an amount of axial displacement occurring all over the specimen. The purpose of installation of a strain gauge for steel is to observe changes in strain at local buckling of steel plates, and the purpose of installation of a strain gauge for encased concrete is to measure ultimate strain when concrete reaches the maximum compressive strength.

3. Experimental results and analysis

3.1 Fracture pattern

As lateral concrete was fractured immediately after all specimens using SM 490 steel reached the

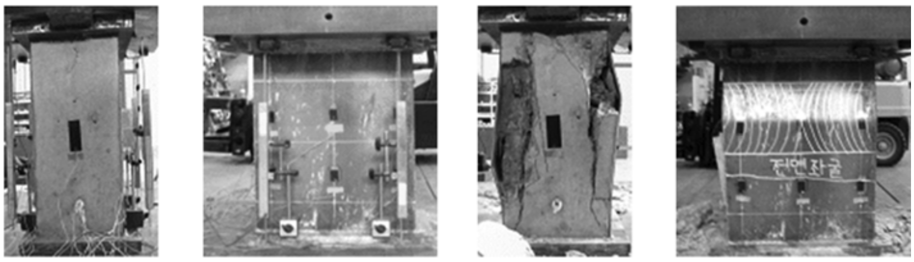

Fig. 4 Shape before/after fracture of the SS400-M specimen

Table 4 Buckling load of the unstiffened steel plates and the comparison (kN)

No.	Specimen	Constraining factor (ξ)	Width ratio (β)	Maximum load P_{test}	Buckling load $P_{buckling}$		$P_{buckling}/P_{test}$	
					Center value	Full value	Center value	Full value
col(1)	col(2)	col(3)	col(4)	col(5)	col(6)	col(7)	col(8)	col(9)
1	SS400-S	0.32	1.27	6282	5085	5120	0.81	0.82
2	SS400-M	0.32	1.60	7051	5440	5665	0.77	0.80
3	SS400-L	0.32	2.27	8956	3850	3850	0.43	0.43
4	SM490-S	0.49	1.27	6562	5110	5084	0.78	0.77
5	SM490-M	0.49	1.60	8069	5616	5452	0.70	0.68
6	SM490-L	0.49	2.27	8850	2986	3031	0.34	0.34
Average value		-	-	-	-	-	0.64	0.64
Standard deviation		-	-	-	-	-	0.20	0.20

Table 5 Comparison of initial stiffness among specimens (kN/mm)

No.	Specimen	Constraining factor (ξ)	Width ratio (β)	Initial stiffness			Remarks		
				Experimental value	Analytical value	Theoretical value	$\frac{col(5)}{col(6)}$	$\frac{col(5)}{col(7)}$	$\frac{col(6)}{col(7)}$
col(1)	col(2)	col(3)	col(4)	col(5)	col(6)	col(7)	col(8)	col(9)	col(10)
1	SS400-S	0.32	1.27	7089	8661	8596	0.82	0.82	1.01
2	SS400-M	0.32	1.60	5388	7604	7186	0.71	0.75	1.06
3	SS400-L	0.32	2.27	7865	7881	7692	1.00	1.02	1.02
4	SM490-S	0.49	1.27	7774	8445	8596	0.92	0.90	0.98
5	SM490-M	0.49	1.60	8241	8199	7186	1.01	1.15	1.14
6	SM490-L	0.49	2.27	6174	7737	7692	0.80	0.80	1.01
Average		-	-	-	-	-	0.87	0.91	1.04
Standard deviation		-	-	-	-	-	0.12	0.15	0.06

maximum compressive strength, the experiment was finished. However, for all specimens with SS 400 steel, as they reached the maximum compressive strength, their load decreased to some degree, lateral concrete was fractured, and the experiment was finished. Fig. 4 shows buckling shapes of the SS400-M specimen before and after the experiment. Fig. 4 (b) shows peeled lateral concrete and buckled steel plates. Buckling of steel plates occurred between studs. This was similar to the buckling shape of steel plates by finite element analysis as described in Section 4 (Fig. 8).

Maximum load and buckling load of each specimen are as described in Table 4. In Table 4, with a constraining factor (ξ) changed from 0.32 into 0.49, when buckling of steel plates was expressed in a ratio of buckling strength of the steel plate to the maximum compressive strength, the ratio decreased (0.96, 0.91, 0.77) as the specimen size increased. In the effect of the yield strength of the steel plates, the maximum compressive strength was slightly increased by the increment of the yield strength under the condition of no change of the cross section and compressive strength of concrete. It was found that when the parameter width ratio (β) was 1.27, 1.60 and 2.27, the steel plate was buckling at about 80%, 74%, and 38% of maximum compressive strength respectively. The higher width ratio (β) was, the earlier the steel plate buckled, and the steel plate displayed ductile behavior until it reached fracture load.

3.2 Initial stiffness

Fig. 6 shows curves of load and strain measured for the U.T.M, the LVDT, the gauges for steel plates and concrete, which are installed at each specimen. It was revealed that buckling of steel plates did not occur up to about 30% of the maximum compressive strength for all the specimens. Both the LVDT and the gauges showed nearly the same strain. Therefore in this study, the experimental initial stiffness was calculated with load of the U.T.M at 30% of the maximum compressive strength and displacements of the LVDT. That is as shown in Eq. (3). The theoretical initial stiffness was calculated using Eq. (4). The initial stiffness of each specimen was as shown in Table 5. The experimental initial stiffness (Eq. (3); col(5)), the analytical initial stiffness (col(6)) based on finite element analysis, and the theoretical initial stiffness (Eq. (4); col(7)) are also shown. As seen from Table 5, the ratio of experimental value to analytical value (col(8)) is 0.87 on an average, that of experimental value to theoretical value (col(9)) is 0.91, and that of analytical value to theoretical value (col(10)) is 1.04. As seen from this result, for initial stiffness, analytical value and theoretical value were found to be most similar, because experimental initial stiffness had large deviation due to inhomogeneity of concrete material, execution errors, and other factors. As a result, a ratio of experimental value to analytical value (col(9)) ranged from 0.75~1.15, and standard deviation was 0.15.

$$K_e = \frac{P_{0.3}}{\delta_{0.3}} \tag{3}$$

$$K_c = \frac{E_c \times A_e}{h} \tag{4}$$

$$A_e = A_c + A_s \times \frac{E_s}{E_c} \times A_{ss} \times \frac{E_{ss}}{E_c} \tag{5}$$

where, E_s : Modulus of elasticity of steel, (N/mm^2)
E_c : Modulus of elasticity of concrete, (N/mm^2)

3.3 Ductility index

It is reported that CFT column generally shows gradual ductility capacity even at the maximum load level without any brittle failure according to the variations of the constraining factor (ξ). However, a USC structure, the subject of this study, has front and rear concrete confinement by front and rear steel plates but does not have any lateral steel plate, thus lateral concrete confinement is impossible. Therefore, as lateral concrete went through brittle fracture as shown in Fig. 4 (b), the experiment was finished. Like this, contrary to existing CFT columns, ductility index was used to see what pattern does ductility capacity of USC structure display. L-H Han (Han 2002) conducted comparative analysis on ductility capacity of a square-shape CFT column according to a constraining factor (ξ) and a width ratio (β) with ductility index as shown in Eq. (6). According to the results of his study, the higher constraining factor (ξ) was and the lesser the width ratio (β) was, the higher ductility index was.

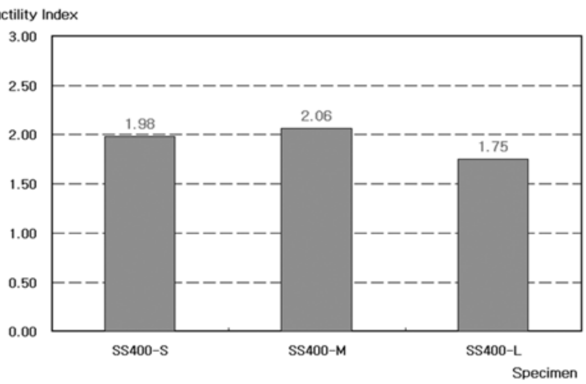

Fig. 5 Ductility index by specimen

$$DI = \frac{\varepsilon_{85\%}}{\varepsilon_y} \tag{6}$$

where, $\varepsilon_{85\%}$: the axial strain when the load falls to 85% of the ultimate load

ε_y : equal to $\varepsilon_y = \dfrac{\varepsilon_{75\%}}{0.75}$

$\varepsilon_{75\%}$: the axial strain when the load attains 75% the ultimate load in the pre-peak stage

Fig. 5 shows the results of comparative analysis on ductility index just for the specimens of SS400 series except those of SM490 series. The reason for exception of the specimens of SM490 series is as mentioned below. The higher the constraining factor (ξ) is, the higher the concrete triaxial stress by steel plates is. Accordingly, the specimens of SM490 series generate more concrete triaxial stress compared to SS400 series. However, a USC structure without lateral steel plate, which is the subject of this study, only had front and rear steel plates therefore as concrete confinement was released laterally and concrete went through brittle fracture with peeling immediately after maximum compressive strength was reached, and consequently ductility index (DI) could not be calculated as shown in Eq. (6). For this reason, just the specimens of SS400 series whose constraining factor (ξ) was 0.32 showed ductility index as shown in Fig. 5. Here, it was found that the SS400-M and SS400-S specimens had nearly same ductility index (DI) but the SS400-L specimen had 0.23 and 0.31 less ductility index (DI) than the SS400-M and SS400-S specimens. The specimen without lateral steel plate showed that the higher the width ratio (β) was, the smaller the ductility index (DI) was, as shown in the result of the L-H Han's study (Han 2002).

3.4 Strain of each material at a compressive load action

Fig. 6 schematizes curves of load versus strain by changes in strain measured at the LVDT, the gauges for steel plates and concrete for each specimen. Also, buckling positions of the steel plate were indicated. Strain measured at the LVDT and the gauges for concrete for all the specimens nearly coincided until the maximum compressive strength was reached by specimen. All the specimens reached the maximum compressive strength when the gauges for concrete reached about 0.003. Among all the specimens, strain of the steel plate nearly coincided with that of the LVDT up to about 30% of the maximum compressive strength. However, with increase in the width ratio (β) as shown in Fig. 4,

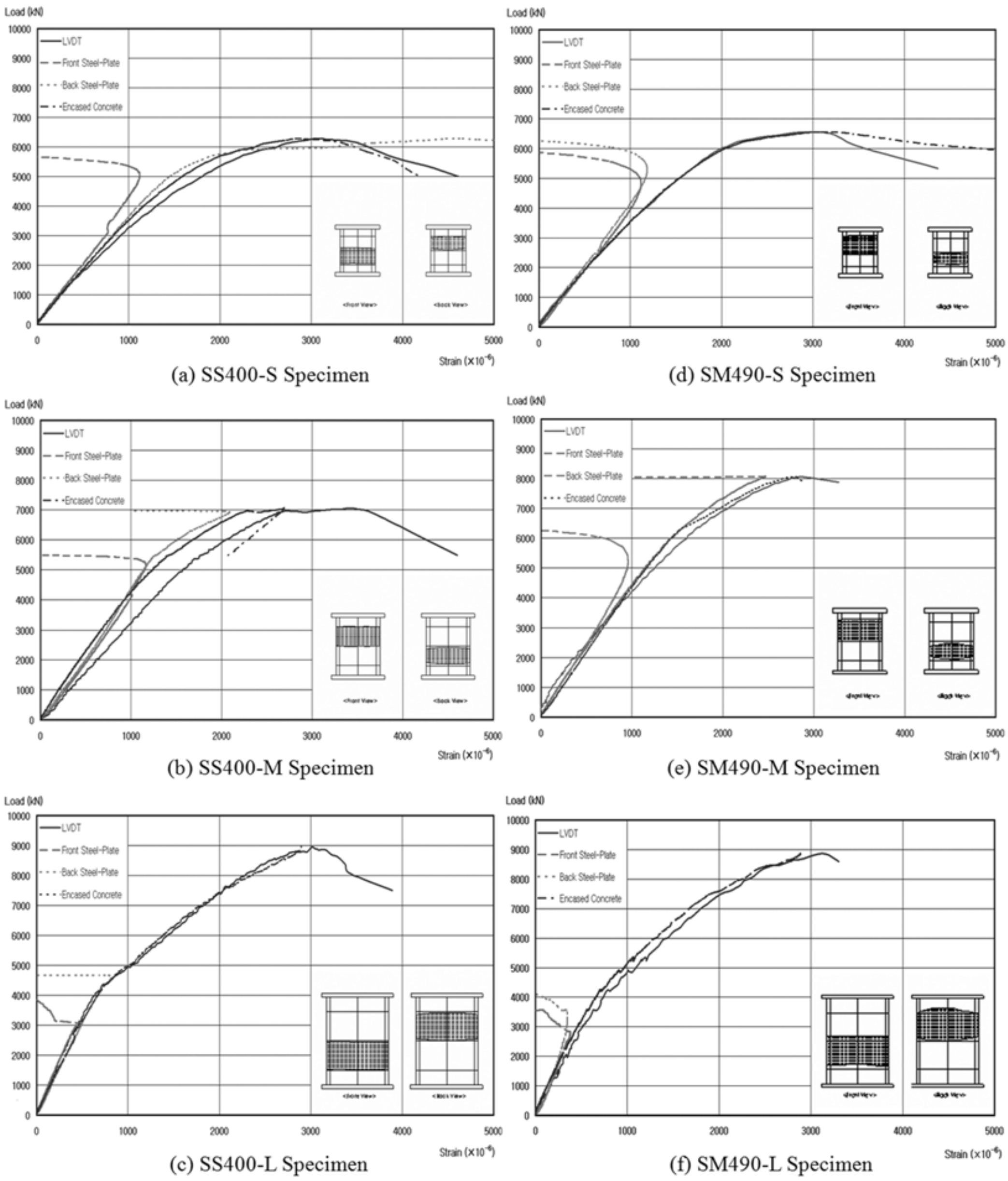

(a) SS400-S Specimen (d) SM490-S Specimen

(b) SS400-M Specimen (e) SM490-M Specimen

(c) SS400-L Specimen (f) SM490-L Specimen

Fig. 6 Load versus strain relation by measuring instrument for each specimen

values of the gauges installed on the surface of the steel plate were suddenly converted from the right to the left as the steel plate was buckled as shown in Fig. 6. On the other hand, B. Uy (Uy 2001) calculated buckling strength of the steel plate using Eq. (7). B. Uy and M.A. Bradford (1996) determined local buckling coefficient (k) of the steel plate to be 10.31 for composite members through many experiments. Here, a Poisson ratio (ν) was set to 0.3. Rearrangement of Eq. (7) on *b* is shown in Eq. (8). Using Eq. (8), effective width of specimens that SS400 and SM490 can exercise by yield strength (F_y)

can be calculated when thickness of steel plate is 6 mm. Here, for SS400 steel, $b = 534$ mm, and for SM490 steel, $b = 454$ mm. Therefore, for the SS400-L and SM490-L specimens, the steel plate is buckled in the elasticity region, as in the actual experiment.

$$\sigma_{01} = \frac{\kappa\pi^2 E_s}{12(1-\nu^2)(b/t)^2} \tag{7}$$

$$b = \sqrt{\frac{\kappa\pi^2 E_s}{12(1-\nu^2)F_y}} \times t \tag{8}$$

4. Finite element analysis

4.1 Material properties

The finite element analysis program used in this study is ABAQUS/CAE(Version6.5). In finite element analysis, for the steel plates, S4R of a shell element was used, and for the stud bolt, a wire element was used. For the plates on the top and bottom of the steel plates, which correspond to flat bearing plates, R3D4 of a rigid element was used. For reduction of analysis time, a rectangular mesh was used. The steel plates and ribs in quadrilateral element shape were selected, and mesh intervals were adjusted as shown in Fig. 7. The characteristics of each material were analyzed with the test results of tension specimens actually used in the experiment. For steel, the plastic behavior was derived with a plasticity option, and to estimate the destruction of concrete, a damaged plasticity option was used for analysis.

4.2 Analysis method

Analysis was conducted in the following order. First, modeling of each element was conducted and material properties were entered. Interaction and contact at constraint were arranged thereafter. Then, the flat bearing plates on the top and bottom of the steel plates were made into rigid plates and constrained

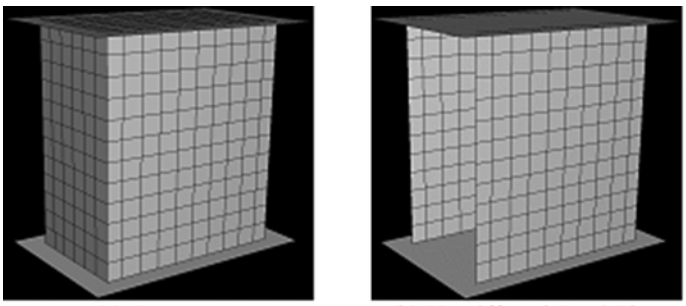

(a) Concrete (b) Unstiffened Steel Plate

Fig. 7 Concrete for finite element analysis and mesh for unstiffened steel plates

(a)CP35/400-T6.0B50 (b)CP35/400-T6.0B33 (c)CP35/400-T6.0B25

Fig. 8 Primary buckling mode of a specimen obtained through finite element analysis(B/t = 50,33,25)

using a tie contact onto concrete, and each nodal point and displacement control point were connected with multiple point constraint so that compressive force can be uniformly delivered. Finally, to examine buckling behavior prior to the experiment, buckling mode was analyzed through buckling analysis. Then a curve of load versus axial displacement was prepared through STATIC-RIKS analysis as shown in Fig. 9.

4.3 Results of analysis

The buckling shape of the unstiffened steel plates, which was obtained through finite element analysis, was bisymmetrical as shown in Fig. 8, and occurred between studs. However, as shown in Fig. 4, it was not bisymmetrical on the actual specimen. It is deemed that such difference originated from an error in making of an actual specimen as well as material inhomogeneity.

The maximum compressive strength of each specimen, which was obtained through finite element analysis, is as shown in Table 6, and curves of load versus axial displacement are as shown in Fig. 9. Seen from Fig. 9, experimental values and analytical values nearly coincided.

5. Examination of compressive strength

This section consists of two subsections. Subsection 5.1 explained various design codes of AISC LRFD in 1999 and 2005, ACI 318 in 2005, and Eurocode 4 in 2004, respectively. Subsection 5.2 compared experimental maximum compressive strength, compressive strength based on finite element analysis of Section 4, and compressive strength based on existing design equations of Subsection 5.1.

5.1 Existing design codes

5.1.1 The 1999 AISC-LRFD

AISC-LRFD (1999) has structural limitations on material strength and thickness of a steel plate. Steel yield strength (F_y) should be less than 415 N/mm^2 and compressive strength (f_c') of normal weight concrete should be more than 21 N/mm^2 and less than 55 N/mm^2. Thickness of a square-shape steel pipe is also limited to $b/t \le \sqrt{3E/F_y}$. Design compressive strength ($\phi_c P_n$) of a square-shape steel pipe is

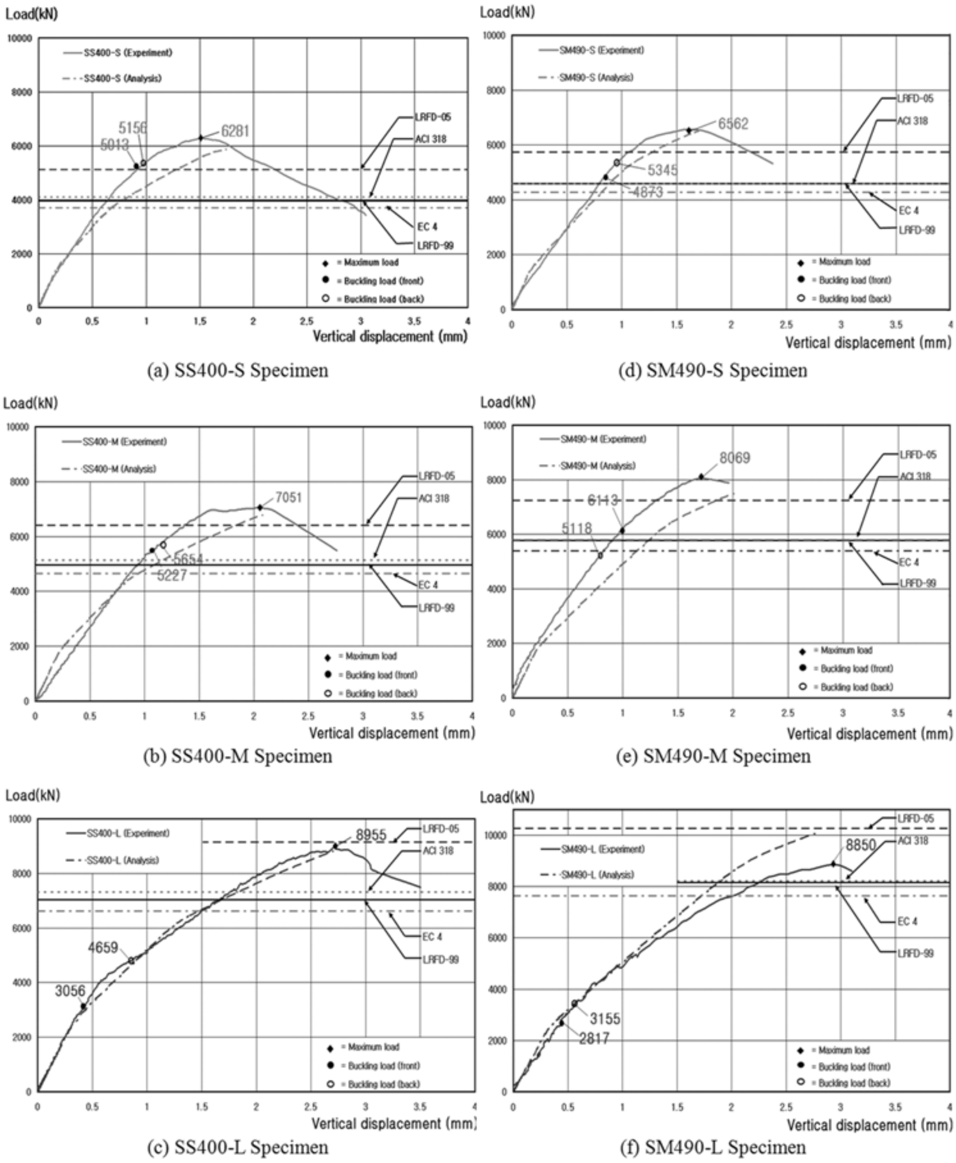

(a) SS400-S Specimen (d) SM490-S Specimen

(b) SS400-M Specimen (e) SM490-M Specimen

(c) SS400-L Specimen (f) SM490-L Specimen

Fig. 9 Load versus axial displacement relation of each specimen

calculated by multiplying cross sectional area of steel by critical compressive strength as shown in Eq. (9). Here, ϕ_c is 0.85.

$$P_n = A_s F_{cr} \tag{9}$$

$$\text{(1) when } \lambda \le 1.5 : F_{cr} = (0.658^{\lambda_c^2}) F_{my} \tag{10}$$

Table 6 Comparison of compressive strength by specimen (kN)

No	Specimen	Experimental value	Analytical value	Theoretical value			
				LRFD-99	LRFD-05	ACI 318	EuroCode 4
col(1)	col(2)	col(3)	col(4)	col(5)	col(6)	col(7)	col(8)
1	SS400-S	6,282	5,851	5,101	5,107	4,085	3,697
2	SS400-M	7,051	6,794	6,405	6,416	5,133	4,647
3	SS400-L	8,956	8,835	9,101	9,138	7,311	6,616
4	SM490-S	6,562	6,520	5,735	5,741	4,593	4,274
5	SM490-M	8,069	7,506	7,220	7,235	5,788	5,388
6	SM490-L	8,850	10,084	10,226	10,274	8,219	7,649

No	Specimen	Experimental value	$\frac{col(3)}{col(4)}$	$\frac{col(3)}{col(5)}$	$\frac{col(3)}{col(6)}$	$\frac{col(3)}{col(7)}$	$\frac{col(3)}{col(8)}$
1	SS400-S	6,282	1.07	1.23	1.23	1.54	1.70
2	SS400-M	7,051	1.04	1.10	1.10	1.37	1.52
3	SS400-L	8,956	1.01	0.98	0.98	1.23	1.35
4	SM490-S	6,562	1.01	1.14	1.14	1.43	1.54
5	SM490-M	8,069	1.08	1.12	1.12	1.39	1.50
6	SM490-L	8,850	0.88	0.87	0.86	1.08	1.16
Average			1.01	1.07	1.07	1.34	1.46
Standard deviation			0.07	0.13	0.13	0.16	0.18

$$\text{(2) when } \lambda > 1.5 : F_{cr} = \left(\frac{0.877}{\lambda_c^2}\right) F_{my} \tag{11}$$

where,

$$\lambda_c = \frac{kL}{r\pi}\sqrt{\frac{F_{my}}{E_m}} \tag{12}$$

$$F_{my} = F_y + C_1 F_{yr}\frac{A_{sr}}{A_s} + C_2 f_c'\frac{A_c}{A_s} \tag{13}$$

(for concrete-filled pipe and HSS : $C_1 = 1$, $C_2 = 0.85$)

$$E_m = E_s + C_3\frac{A_c}{As} \text{ (for concrete-filled and HSS : } C_1 = 0.4) \tag{14}$$

5.1.2 The 2005 AISC-LRFD

AISC-LRFD (2005) also has structural limitations on material strength and thickness of a steel. Steel yield strength (F_y) should be less than 525 N/mm^2 and compressive strength of normal weight concrete (f_c') should be more than 21 N/mm^2 and less than 70 N/mm^2. Thickness of a square-shape steel pipe is also limited to $b/t \le 2.26\sqrt{E/F_y}$. Design compressive strength ($\phi_c P_n$) of a square-shape steel pipe is calculated by the limit state of flexural buckling based on column slenderness as shown in Eqs. (15) and

(16). Here, ϕ_c is 0.75.

$$(1)\ \text{when } P_e \geq 0.44P_0 : P_n = P_0\left[0.658^{\left(\frac{P_0}{P_e}\right)}\right] \tag{15}$$

$$(2)\ \text{when } P_e \geq 0.44P_0 : P_n = 0.877P_0 \tag{16}$$

$$\text{Where, } P_0 = A_sF_y + A_{sr}F_{yr} + C_2A_cf_c' \tag{17}$$

(C_2 = 0.85 for rectangular sections and 0.95 for circular sections)

$$P_e = \pi^2(EI_{eff})/(KL)^2 \tag{18}$$

$$EI_{eff} = E_sI_s + E_sI_{sr} + C_3E_cI_c \tag{19}$$

$$C_3 = 0.6 + 2\left(\frac{A_s}{A_c + A_S}\right) \leq 0.9 \tag{20}$$

5.1.3 The 2005 ACI 318-05

ACI 318-05 also has structural limitations on material strength and thickness of a steel plate. Steel yield strength(F_y) should be less than 350 N/mm^2 and concrete compressive strength(f_c') should be more than 21 N/mm^2. Thickness of a square-shape steel pipe is also limited to $t \leq b\sqrt{f_y/3E_s}$. Compressive strength of a square-shape steel pipe is shown in Eq. (21). Normal compressive strength should be calculated with a reduction factor 0.8 in consideration of minimum flexural moment by accidental eccentricity, and this is shown in Eq. (22).

$$P_0 = F_yA_s + F_{yr}A_{sr} + 0.85f_c'A_c \tag{21}$$

$$P_n = 0.8P_0 \tag{22}$$

where, A_{sr} : Cross-Sectional Area of Reinforcing Bar, (mm^2)
F_{yr} : Yield Strength of Reinforcing Bar, (N/mm^2)

5.1.4 The 2004 Eurocode 4

Compressive strength with plastic resistance of a composite column as provided in Eurocode 4 is shown in Eq. (23). In other words, it is an accumulation of compressive strength of each material divided by a partial safety factor.

$$P_0 = A_sF_y/\gamma_s + A_{sr}F_{yr}/\gamma_s + 0.85A_cf_c'/\gamma_c \tag{23}$$

where, γ_s : the partial safety factor for structural steel (= 1.1)
γ_c : the partial safety factor for structural concrete (= 1.5).

5.2 Comparative analysis of compressive strength

Fig. 9 shows curves of load versus axial displacement for each specimen. Here, the solid lines are from the experiment, while the dotted lines are from finite element analysis. Also, the four horizons indicate normal compressive strength under existing design equations. First, for experimental values, with increase in a width ratio (β) from 1.27 to 2.27, a cross section of the specimen increased, and maximum compressive strength of the specimen also increased from about 6,300kN to 9,000kN. With increase in a constraining factor (ξ) from 0.32 to 0.49, steel yield strength (F_y) increased, and maximum compressive strength of the specimen also increased up to about 5%. Except the specimen SM490-L, all the specimens approximated 100%. The curves of load versus axial displacement obtained from finite element analysis show nearly similar behavior to the curves of load versus axial displacement obtained from the actual experiment.

The most important factor at design of compressive structural members is to examine the maximum compressive strength of compressive structural members. Therefore maximum compressive strength was calculated using the existing equations in subsection 5.1, and it was compared with the experimental maximum compressive strength. The results are shown in Table 6: experimental values (col(3)) obtained from an actual experiment, analytical values (col(4)) obtained from finite element analysis, theoretical values (Eq. (9); col(5)) obtained from AISC-LRFD in 1999, theoretical values (Eq. (15) or Eq.(16);col(6)) obtained from AISC-LRFD in 2005, theoretical values (Eq.(22);col(7)) obtained from ACI 318 in 2005, and theoretical values (Eq. (23);col(8)) obtained from Eurocode 4 in 2004. Seen from Table 6, comparison of experimental values with existing equations in AISC-LRFD of 1999 revealed that a ratio of experimental value to LRFD-99 (col(3)/col(5)) is 0.87~1.23, with average of 1.07, and standard deviation of 0.13. Comparison of experimental values with existing equations in AISC-LRFD of 2005 revealed that a ratio of experimental value to LRFD-05 (col(3)/col(6)) is 0.86~1.23, with average of 1.07, and standard deviation of 0.13. Comparison of experimental values with existing equations in ACI 318 of 2005 revealed that a ratio of experimental value to ACI 318 (col(3)/col(7)) is 1.08~1.54, with average of 1.34, and standard deviation of 0.16. Finally, comparison of experimental values with existing equations in Eurocode 4 of 2004 revealed that a ratio of experimental value to Eurocode 4(col(3)/col(8)) is 1.16~1.70, with average of 1.46, and standard deviation of 0.18.

Therefore it is deemed that the calculation of maximum compressive strength based on AISC-LRFD of 2005 is significantly reliable. However, in the specimen SM490-L, the experimental value was shown to be about 15% less than the theoretical value from AISC-LRFD of 2005. At calculation of maximum compressive strength of AISC-LRFD of 2005, compressive strength was reduced just by a slenderness ratio of compressive members without consideration of execution errors and factors for reduction of material compressive strength, and consequently compressive strength of a short column could not be reduced. However, for ACI 318 and EC 4, a safety factor was given to compressive strength of a short column in a manner of allowing for eccentricity or reducing strength by material.

6. Conclusion

In this study, a comparative analysis was conducted on fracture pattern, initial stiffness, ductility index, and strain in order to examine the compressive strength characteristics of the unstiffened steel plate concrete(USC) structures without lateral steel plates. The experimental results were verified thorough finite element analysis. Based on the study results, the following conclusions could be drawn:

(1) In case of the buckling shape to the compressive strength of the USC structures, the buckling shape of the specimens occurred to the adjacent studs in lateral direction with the same pattern. This pattern coincides with the buckling shapes from the finite element analysis.

(2) The three types of stiffness including experimental, analytical, and theoretical values are well agreed among them. Comparing the experimental stiffness, the analytical stiffness, and the theoretical stiffness in terms of numerical values, the ratio of the analytical to the theoretical values and standard deviation were 1.04 and 0.06, respectively. The ratio of the experimental to the theoretical values and standard deviation were 0.91 and 0.15, respectively. That is better coincidence in the initial stiffness was found rather the one between analytical and theoretical values than the one between experimental and theoretical values.

(3) In the specimens without the lateral steel plates, as a constraining factor (ξ) became higher, the lateral concrete generated relatively huge peeling and went through brittle fracture. The ductility index (DI) was decreased with the increase of the width ratio (β) which is normally increased by the width rather than the thickness.

(4) The axial strain was 0.003 when all the specimens reached the maximum compressive strength. At the same time, the concrete strain reached 0.003 which implies that it nearly coincides with the axial strain of the specimen itself. On the other hand, in the specimen with large β the strain of the steel plate gradually changed from compression into tension in elasticity region.

(5) The comparative studies of the maximum compressive were performed to study the compression behavior in terms of the experimental values, analytical values, and values from existing design codes. Then experimental values and analytical values nearly coincided, and the values acquired from the existing equations showed a safety margin by 7% compared to experimental values.

Acknowledgements

This study was performed by the funding of the Power Industry Research & Development Project in 2006, which is entitled "Technological Development of a Module for Structures of Nuclear Power Plants(SC structure)", and the authors are grateful for this support.

References

ABAQUS, Inc (2004), *ABAQUS Standard User's Manual*, ABAQUS Version 6.5.

American Concrete Institute (ACI) (2005), *Building Code Requirements for Structural Concrete*, American concrete Institute, Detroit.

American Institute of Steel Construction (AISC) (2005), *Load and resistance factor design specification for structural steel buildings*, American Institute of Steel Construction, Inc, Chicago.

British Standards Institution (2004), Eurocode 4, "Design of Composite steel and Concrete Structures, Part 1.1: General Rules and Rules for Building", DD-ENV 1994-1-1, London.

Choi, B.J., *et al.* (2008), "Compression Tests for Unstiffened Steel Plate-Concrete Structures with Variation of B/t Ratio", *J. Kor. Soc. Steel Constr.*, **20**(4), 549-559.

Corus (2003), *Bi-Steel Design & Construction Guide*, 2nd Edition.

Corus (2004), *An introduction to the Corefast system*, www.corusconstruction.com.

Corus (2006), *Corefast selected for new 18-storey Birmingham tower*, www.bi-steel.com/news.

Han, L.H. (2002), "Tests on stub columns of concrete-filled RHS sections", *J. Constr. Steel. Res*., **58**(3), 353-372.

Han, L.H., Zhao, X.L. and Tao, Z. (2001), "Tests and mechanics model for concrete-filled SHS stub columns, columns and beam-columns", *Steel Compos. Struct.*, **1**(1), 51-74.

JEAG 4618 (2005), *Technical Guidelines for Seismic Design of Steel Plate Concrete Structures: for Buildings and Structures.*

Kanchi, M., *et al.* (1996), "Experimental Study on A Concrete Filled Steel Structure, Part 2., Compressive Test (1)", *Architectural Institute of Japan Conf.*, pp 1071-1072.

Liang, Q.Q., Uy, B. and Richard Liew, J.Y. (2006), "Nonlinear analysis of concrete-filled thin-walled steel box columns with local buckling effects", *J. Constr. Steel. Res.*, **62**(6), 581-591.

Miyauchi, Y., *et al.* (1996), "Experimental Study on A Concrete Filled Steel Structure, Part 3 Compressive Test (2)", *Architectural Institute of Japan Conf*., pp 1073-1074.

Saadeghvaziri, M.A. and Shams, M. (1997), "Nonlinear Modeling and Evaluation of Concrete-Filled Steel Tubular Columns", *ABAQUS Users Conf. Proc*., **6**, 667-680.

Shams, M. and Saadeghvaziri, M.A. (1999), "Nonlinear Response of Concrete-filled Steel Tubular Columns Under Axial Loading", *ACI Struct. J.*, **96**(7), 1009-1017.

Tao, Z., Han, L.H. and Wang, D.Y. (2008), "Strength and ductility of stiffened thin-walled hollow steel structural stub columns filled with concrete", *Thin-Wall. Struct.*, **46**(10), 1113-1128.

Uy, B. (2001), "Strength of short concrete filled high strength steel box columns", *J. Constr. Steel. Res*., **57**(2), 113-134.

Uy, B. and Bradford, M.A. (1996), "Elastic local buckling of steel plates in composite steel-concrete members", *Eng. Struct*., **18**(3), 193-200.

Vrcelj, Z. and Uy, B. (2002), "Strength of slender concrete-filled steel box columns incorporating local buckling", *J. Constr. Steel. Res*., **58**(2), 275-300.

CC